# BAYESIAN JOINT SUPER-RESOLUTION, DECONVOLUTION, AND DENOISING OF IMAGES WITH POISSON-GAUSSIAN NOISE

*Q. Gao*[1,2], *S. Eck*[2], *J. Matthias*[3], *I. Chung*[4], *J. Engelhardt*[3], *K. Rippe*[4], *and K. Rohr*[2]

[1] CellNetworks, Heidelberg University, Germany
[2] Biomedical Computer Vision Group, Dept. Bioinformatics and Functional Genomics,
BioQuant, IPMB, Heidelberg University and DKFZ Heidelberg, Germany
[3] Dept. Optical Nanoscopy, MPI for Medical Research, Heidelberg, Germany
[4] Division of Chromatin Networks, DKFZ and BioQuant, Heidelberg, Germany

## ABSTRACT

For images degraded by significant noise with mixed Poisson-Gaussian (PG) statistics, deconvolution or denoising methods generally do not perform well if they consider only one type of noise. We propose a novel method in a Bayesian framework that simultaneously performs deconvolution, denoising as well as super-resolution, to restore images with mixed PG noise. Our model is based on a likelihood modeling the statistics of PG noise, and a generative Markov random field image prior. We approximate the likelihood using mixtures of Gaussians, which allows defining a block Gibbs sampler for efficient inference. The degraded images are restored through a sampling-based scheme to approximate the Bayesian minimum mean squared error estimate. We have applied our method to different types of synthetic images and real images from a STED microscope. Experiments show that our method can compete with state-of-the-art approaches.

***Index Terms***— Super-resolution, Deconvolution, Denoising, Poisson-Gaussian Noise, Fluorescence Microscopy Images

## 1. INTRODUCTION

Images acquired by photon-counting devices in applications such as biology, medicine, and astronomy are usually degraded by noise with mixed Poisson-Gaussian (PG) statistics and by blurring characterized by the system point spread function. In previous work, besides denoising methods dedicated to PG noise (*e.g.*, [1, 2, 3]), methods for joint deconvolution and PG denoising (*e.g.*, [4, 5, 6, 7, 8, 9]) have been proposed. Recently, Gazagnes *et al*. [10] proposed a joint super-resolution and denoising method for single-molecule localization microscopy (SMLM). However, there Poisson noise is treated as additive Gaussian noise (by using a quadratic data fidelity term).

Most of the methods mentioned above are formulated within a maximum a posteriori (MAP) framework [3, 4, 5, 6, 7, 10]. To achieve best performance, a regularization parameter which defines the trade-off between the data fidelity term and the regularization term must be tuned manually. In contrast to MAP, [1] and [8] avoid such problem by approximating the minimum mean square error (MMSE) estimate. More recently, Marnissi *et al*. [9] proposed a Bayesian deconvolution method that computes the MMSE estimate and the regularization parameter through variational Bayesian approximation. In general, the usage of an application-dependent regularization parameter suggests that common regularizers (*e.g.*, total variation) employed in these MAP-based methods as well as in [9] are insufficient as a generative image prior.

A Bayesian MMSE estimate, which is computed based on the whole model distribution, exploits more information and is statistically more sound than an MAP estimate. However, computing the MMSE estimate is generally difficult for non-convex problems. In methods for denoising and deblurring for additive Gaussian noise [11, 12], a trained non-convex probabilistic generative image prior is used and the MMSE estimate is approximated by averaging model samples based on an efficient block Gibbs sampler. As the MMSE estimation operates in a purely generative setting, a regularization parameter is not needed. However, this efficient Gibbs sampler cannot handle the case of PG noise due to the more complex statistics.

In this paper, we propose a Bayesian deconvolution and denoising model for mixed Poisson-Gaussian noise and determine the MMSE solution. We explore the statistics of PG noise and find that its distribution can be well approximated using mixtures of Gaussians (MoGs). A generative high-order Markov random field (MRF) image prior in [13] is employed and a regularization parameter is not needed. The MoG-based likelihood (data fidelity) and the Gaussian scale mixture (GSM)-based prior allow to augment the model using hidden variables and define an efficient block Gibbs sampler. The degraded images are restored using the MMSE estimate that is approximated by averaging multiple samples from

our probabilistic model. We also integrate super-resolution into our model framework and simultaneously achieve super-resolution, deconvolution, and denoising. We have applied our approach to different types of synthetic data and performed a comparison with previous methods. Experiments demonstrate that our joint method is superior to a sequential scheme, and that the deconvolution performance can compete with state-of-the-art methods. Our method is also applied to real microscopy images of telomeres acquired via stimulated emission depletion (STED) nanoscopy.

## 2. METHOD

### 2.1. Model formulation

We formulate image restoration from a single image based on the posterior distribution in a Bayesian framework

$$p(\mathbf{x}|\mathbf{y}) \propto p_L(\mathbf{y}|\mathbf{x}; \boldsymbol{\Theta}) \cdot p_P(\mathbf{x}; \boldsymbol{\Omega}), \quad (1)$$

where $\mathbf{y} \in \mathbb{R}^N$ is the given degraded image (noisy, blurry, low-resolution), $\mathbf{x} \in \mathbb{R}^{r^2 N}$ is the image to be restored (with a scaling factor $r$ in case of super-resolution), and $\boldsymbol{\Theta}$ and $\boldsymbol{\Omega}$ are the likelihood and prior parameters, respectively.

**The likelihood model.** For the case of Poisson-Gaussian noise, the intensity of each pixel $y_i$ of the observed image $\mathbf{y}$ can be modeled as $y_i = \alpha t_i + n_i$, where $t_i$ follows a Poisson distribution

$$t_i \sim \mathrm{Po}\left(\tfrac{1}{\alpha}(\mathbf{S}(\mathbf{k}*\mathbf{x}))_i\right) = \mathrm{Po}\left((\tfrac{1}{\alpha}\mathbf{H}\mathbf{x})_i\right) := \mathrm{Po}(\tilde{x}_i), \quad (2)$$

and $\mathbf{H}$ is the matrix representing the convolution of $\mathbf{x}$ with some point spread function $\mathbf{k}$ and down-sampling by $\mathbf{S} \in \mathbb{R}^{N \times r^2 N}$, $\alpha$ is a gain factor that controls the Poisson noise strength, and $n_i \sim \mathcal{N}(\mu_n, \sigma_n^2)$ is additive Gaussian noise.

We assume that pixels in $\mathbf{y}$ are conditionally independent. The likelihood model can then be written as

$$
\begin{aligned}
p_L(\mathbf{y}|\mathbf{x}; \boldsymbol{\Theta}) &= \prod_i p(y_i|\tilde{x}_i) \\
&= \prod_i \left( \sum_{t_i=0}^{+\infty} p(y_i|t_i) \cdot p(t_i|\tilde{x}_i) \right) \\
&= \prod_i \left( \sum_{t_i=0}^{+\infty} \frac{e^{-\frac{(y_i - \alpha t_i - \mu_n)^2}{2\sigma_n^2}}}{\sqrt{2\pi}\sigma_n} \frac{\tilde{x}_i^{t_i} \cdot e^{-\tilde{x}_i}}{t_i!} \right).
\end{aligned} \quad (3)
$$

**The prior model.** We use the filter-based, high-order Markov random field (MRF) image prior in [13]:

$$p_P(\mathbf{x}; \boldsymbol{\Omega}) \propto \prod_i \prod_k \psi\big((\mathbf{f}_k * \mathbf{x})_i; \boldsymbol{\omega}_k\big), \quad (4)$$

where $\mathbf{f}_k$ are linear filters and "$*$" denotes convolution. Filter-specific functions $\psi(\cdot; \boldsymbol{\omega}_k)$ with parameters $\boldsymbol{\omega}_k$ are potential functions represented by Gaussian scale mixtures (GSMs)

$$\psi(\cdot; \boldsymbol{\omega}_k) = \sum_{j=1}^{W} \omega_{kj} \cdot \mathcal{N}\big(0, s_j \cdot \sigma_k^2\big), \quad (5)$$
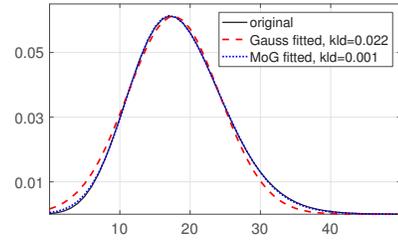


**Fig. 1**. Likelihood values $p(y_i|\tilde{x}_i)$ of (7) w.r.t. $\tilde{x}_i$ (black, solid) for $y_i = 20$ with $\alpha = 2$, $\mu_n = -15$, and $\sigma_n = 10$. Model fitting using a mixture of Gaussians with three components (blue, dotted) is more accurate than using a Gaussian (red, dashed). "kld" means KL-divergence (a smaller value corresponds to a better fit).

where $\omega_{kj} > 0, \sum_j \omega_{kj} = 1$ are the mixture weights of the zero-mean Gaussian components with scales $s_j$ and base variance $\sigma_k^2$. The model parameters $\boldsymbol{\Omega} = \{\mathbf{f}_k, \omega_{kj}\}$ (filters and GSM weights) can be learned unsupervisedly from training images (see [13] for details on the learning procedure).

### 2.2. Sampling-based inference

To restore the image $\mathbf{x}$ from the degraded image $\mathbf{y}$, we use the Bayesian minimum mean squared error (MMSE) estimate $\hat{\mathbf{x}}$:

$$\arg\min_{\hat{\mathbf{x}}} \int \|\hat{\mathbf{x}} - \mathbf{x}\|^2 p(\mathbf{x}|\mathbf{y}; \boldsymbol{\Theta}, \boldsymbol{\Omega}) d\mathbf{x} = E[\mathbf{x}|\mathbf{y}], \quad (6)$$

which is equivalent to the mean of the posterior distribution (1). As there is no closed form expression for the MMSE estimate of our model, we use a sampling-based approximation.

Given $\mathbf{y}$, the likelihood $p(y_i|\tilde{x}_i)$ is a function of $\tilde{x}_i$, which has an asymmetric bell shape (Fig. 1, the black solid curve). We can well approximate the model likelihood by fitting these functions using general mixtures of Gaussians (MoGs):

$$p\big(y_i|\tilde{x}_i\big) \propto p(\tilde{x}_i; y_i) = \sum_{j=1}^{M} \pi_{y_i j} \cdot \mathcal{N}\big(\tilde{x}_i; \tilde{\mu}_{y_i j}, \tilde{\sigma}_{y_i j}^2\big), \quad (7)$$

where $\pi_{y_i j} > 0$, $\tilde{\mu}_{\cdot j}$ and $\tilde{\sigma}_{\cdot j}^2$ are the means and variances of the Gaussian components, respectively. Since in practice the value of $y_i$ is usually within a finite set (or can be discretized for real values), the Gaussian mixture parameters can be obtained in advance before inference. Note that (7) is different to the Gaussian scale mixture models in (5).

In [11, 12], the scales of the GSMs in (5) are retained as hidden random variable $z_{ik} \in \{1, ..., W\}$ such that $p(\mathbf{x}; \boldsymbol{\Omega}) = \sum_{\mathbf{z}} p(\mathbf{z}, \mathbf{x}; \boldsymbol{\Omega})$, allowing to define a rapidly mixing auxiliary-variable Gibbs sampler. In our case, we further augment the mixture model in (7) using the hidden variable $h_i \in \{1, ..., M\}$, which represents the index of the Gaussian mixture component, such that $p(\mathbf{x}; \mathbf{y}) = \sum_{\mathbf{h}} p(\mathbf{h}, \mathbf{x}; \mathbf{y})$. The following conditional distributions can be derived

$$p(h_i|\mathbf{x}, y_i) \propto \pi_{y_i h_i} \cdot \mathcal{N}\big((\tfrac{1}{\alpha}\mathbf{H}\mathbf{x})_i; \tilde{\mu}_{y_i h_i}, \tilde{\sigma}_{y_i h_i}^2\big), \quad (8)$$

$$p(z_{ik}|\mathbf{x}) \propto \omega_{kz_{ik}} \cdot \mathcal{N}\big((\mathbf{f}_k * \mathbf{x})_i; 0, s_{z_{ik}}\sigma_k^2\big), \quad (9)$$

**Algorithm 1** Sampling-based MMSE estimate approximation

1:  initialization of $\mathbf{x}^{(0)} \in \mathbb{R}^{r^2 N}$;
2:  **for** $t = 1, 2, \ldots$ **do**
3:      sample $\mathbf{h}^{(t)} \sim p(\mathbf{h}|\mathbf{x}^{(t-1)}, \mathbf{y})$ according to (8);
4:      sample $\mathbf{z}^{(t)} \sim p(\mathbf{z}|\mathbf{x}^{(t-1)})$ according to (9);
5:      update $\mathbf{b}^{(t)}$, $\mathbf{Q}^{(t)}$ and $\boldsymbol{\Sigma}^{(t)}$ in (10);
6:      sample $\mathbf{x}^{(t)} \sim p(\mathbf{x}|\mathbf{z}^{(t)}, \mathbf{h}^{(t)}, \mathbf{y})$ according to (10);
7:      **if** $t > B$ **then**    ▷ $B$: no. of burn-in iterations
8:          compute $\hat{\mathbf{x}}^{(t)} = \frac{1}{t-B} \sum_{i=B+1}^{t} \frac{1}{\alpha} \boldsymbol{\Sigma}^{(i)} \mathbf{H}^T \mathbf{Q}^{(i)} \mathbf{b}^{(i)}$;
9:          **if** $\|\hat{\mathbf{x}}^{(t)} - \hat{\mathbf{x}}^{(t-1)}\| \leqslant \epsilon$ **then**
10:             **return** $\hat{\mathbf{x}}^{(t)}$;

$$
\begin{aligned}
p(\mathbf{x}|\mathbf{z}, \mathbf{h}, \mathbf{y}) &\propto p(\mathbf{y}|\mathbf{x}, \mathbf{h}) \cdot p(\mathbf{x}|\mathbf{z}) \\
&\propto \prod_i \mathcal{N}\big((\tfrac{1}{\alpha}\mathbf{Hx})_i; \mu_{y_i h_i}, \sigma^2_{y_i h_i}\big) \\
&\quad \cdot \prod_i \prod_k \mathcal{N}\big(\mathbf{f}_{ik}^T \mathbf{x}; 0, s_{z_{ik}} \sigma_k^2\big) \qquad (10)\\
&\propto \mathcal{N}\big(\tfrac{1}{\alpha}\mathbf{Hx}; \mathbf{b}, \mathbf{Q}^{-1}\big) \cdot \mathcal{N}\big(\mathbf{x}; 0, \mathbf{P}^{-1}\big) \\
&\propto \mathcal{N}\big(\mathbf{x}; \tfrac{1}{\alpha}\boldsymbol{\Sigma}\mathbf{H}^T\mathbf{Q}\mathbf{b}, \boldsymbol{\Sigma}\big),
\end{aligned}
$$

where $\mathbf{f}_{ik}$ is defined as $\mathbf{f}_{ik}^T \mathbf{x} = (\mathbf{f}_k * \mathbf{x})_i$, $\mathbf{b} = [..., \tilde{\mu}_{y_i h_i}, ...]^T$, $\mathbf{Q} = \text{diag}\{1/\tilde{\sigma}^2_{y_i h_i}\}$, $\mathbf{P} = \sum_i \sum_k \frac{1}{s_{z_{ik}} \sigma_k^2} \mathbf{f}_{ik} \mathbf{f}_{ik}^T$ and $\boldsymbol{\Sigma} = \big(\frac{1}{\alpha^2} \mathbf{H}^T \mathbf{Q} \mathbf{H} + \mathbf{P}\big)^{-1}$.

We can then define a rapidly mixing block Gibbs sampler that alternatively samples $\mathbf{h}, \mathbf{z}$, and $\mathbf{x}$ according to Eqs. (8, 9, 10) respectively, which is very efficient as (8) and (9) are discrete distributions conditionally independent to each other given $\mathbf{y}$ and (10) is a multivariate Gaussian that can be sampled through solving a linear system of equations. The MMSE estimate $\hat{\mathbf{x}}$ can be approximated by averaging multiple samples of $\mathbf{x}$. To achieve faster convergence, instead we average the conditional expectations from (10) during Gibbs sampling, which is called Rao-Blackwellized estimation [14]. Algorithm 1 provides the pseudo-code of the sampling-based MMSE estimate approximation. Note that it is straightforward to parallelize sample drawing by running multiple samplers, which can further greatly improve the efficiency of inference.

## 3. EXPERIMENTS

We applied our method to both natural images and fluorescence microscopy images. For the prior model, we use the $3 \times 3$ MRF with 8 filters learned from natural images in [13]. We also studied retraining the parameters using fluorescence microscopy images. However, it turned out that this does not improve the result. The reason is probably that microscopy images have similar local image structures as natural images. For the likelihood model, unless otherwise mentioned, we use MoGs with three components. Image noise parameters $\alpha$, $\mu_n$, $\sigma_n$ and $\mathbf{H}$ are assumed to be given (for synthetic data) or are estimated from the images. No additional parameters need to be tuned. For a performance comparison, we choose popu-

**Table 1**. Denoising results (PSNR in dB) for test images with different noise parameters.

| Poiss. param. $\alpha$ | 1 | | 2 | | 5 | |
|---|---|---|---|---|---|---|
| Gauss. param. $\sigma_n$ | 10 | 20 | 10 | 20 | 10 | 20 |
| Method | *Crym* $256 \times 256$ | | | | | |
| Noisy input | 25.74 | 21.59 | 24.22 | 20.97 | 21.53 | 19.56 |
| PURE-LET [1] | 29.77 | 27.31 | 28.84 | 26.95 | 27.23 | 26.09 |
| Ours ($M=1$) | 29.83 | 27.36 | 28.84 | 26.97 | 27.09 | 26.05 |
| Ours ($M=3$) | **29.87** | **27.39** | **28.90** | **27.01** | **27.27** | **26.14** |
| Method | *Moon* $512 \times 512$ | | | | | |
| Noisy input | 26.13 | 21.99 | 24.51 | 21.31 | 21.69 | 19.76 |
| PURE-LET [1] | 29.67 | 26.85 | 28.77 | 26.56 | 27.34 | 25.92 |
| Ours ($M=1$) | 29.76 | 27.32 | 28.87 | 27.12 | 27.00 | 26.18 |
| Ours ($M=3$) | **29.85** | **27.40** | **28.98** | **27.26** | **27.36** | **26.45** |
| Method | *Fluocells* $512 \times 512$ | | | | | |
| Noisy input | 26.92 | 22.44 | 25.68 | 21.98 | 23.19 | 20.79 |
| PURE-LET [1] | 33.92 | 30.50 | 33.25 | 30.27 | 31.97 | 29.91 |
| Ours ($M=1$) | 34.09 | 31.26 | 33.45 | 31.35 | 31.67 | 30.83 |
| Ours ($M=3$) | **34.18** | **31.36** | **33.56** | **31.44** | **32.12** | **31.00** |



(a) Original  (b) Noisy  (c) PURE-LET [1]  (d) Our method
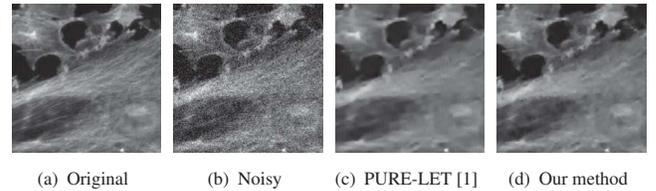
**Fig. 2**. Restoration of *Fluocells* (cropped) degraded by PG noise ($\alpha=5, \mu_n=0, \sigma_n=20$).

lar denoising and deconvolution methods with authors' code available.

**Denoising.** In this case, $\mathbf{H}$ is set to an identity matrix. As can be seen from Tab. 1, using mixtures of Gaussians (3 components) for likelihood approximation yields a gain of the peak signal-to-noise ratio (PSNR) up to $0.45$dB compared to a single Gaussian, which suggests that the accuracy of likelihood modelling is crucial for the performance. Our method outperforms the popular Poisson-Gaussian denosing method PURE-LET [1] and generates less artifacts in the restored images, especially when the noise strength is large (see Fig. 2).

**Deconvolution.** Here $\mathbf{H}$ is a convolution matrix generated from a blur kernel. Tab. 2 and Fig. 3 show that our method outperforms GILAM [15], which is a deconvolution method for Poissonian images. GILAM fails when the Gaussian noise part of the PG noise gets stronger. Compared to the method in [5] (using their settings), our method is slightly better (less outlier pixels in the restored image, see Fig. 4).
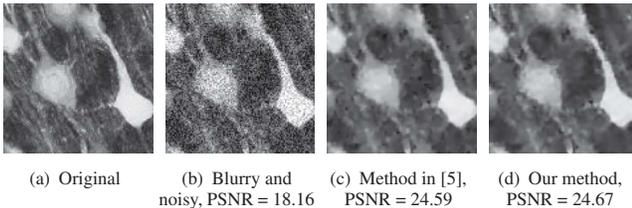
**Super-resolution.** When using a Gaussian blurring and downsampling matrix for $\mathbf{H}$, our method can perform super-resolution and denoising simultaneously. Fig. 5 shows a comparison of our joint scheme and a sequential scheme of denoising (our method with $\mathbf{H}$ as identity matrix) followed by bicubic interpolation. It can be seen that our joint scheme yields sharper image edges.

**Table 2**. Deconvolution results (PSNR in dB) for Gaussian blur with variance 3 and different noise parameters.

| Pois. param. $\alpha$ | 1 | | 5 | |
|---|---|---|---|---|
| Gaus. param. $\sigma_\text{n}$ | 0 | 10 | 0 | 10 |
| Method | *Cameraman* $256\times256$ | | | |
| Input | 22.34 | 21.36 | 18.79 | 18.36 |
| GILAM [15] | 25.50 | 23.00 | 23.69 | 23.50 |
| Our method | **25.70** | **25.08** | **24.35** | **24.12** |
| Method | *Crym* $256\times256$ | | | |
| Input | 23.86 | 22.49 | 20.66 | 19.98 |
| GILAM [15] | 25.87 | 22.38 | 23.74 | 23.51 |
| Our method | **26.17** | **25.50** | **24.73** | **24.49** |
| Method | *Fluocells* $512\times512$ | | | |
| Input | 28.92 | 25.84 | 23.87 | 22.72 |
| GILAM [15] | 31.20 | 22.93 | 29.13 | 27.97 |
| Our method | **32.84** | **31.55** | **30.51** | **30.40** |



(a) Original    (b) Blurry and noisy    (c) GILAM [15]    (d) Our method
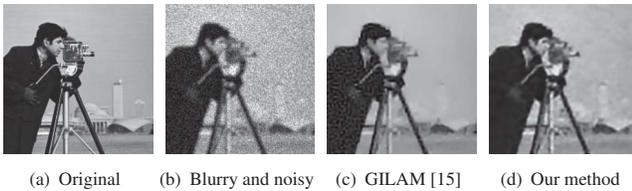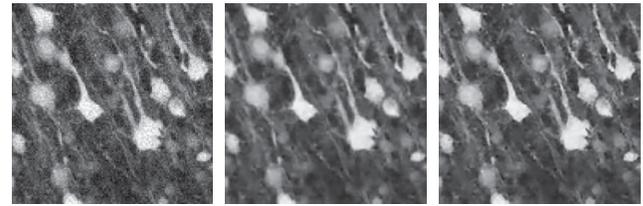
**Fig. 3**. Deconvolution of *Cameraman* (cropped) degraded by Gaussian blur ($\sigma^2=3$) and PG noise ($\alpha=5, \mu_\text{n}=0, \sigma_\text{n}=10$).



(a) Original    (b) Blurry and noisy, PSNR = 18.16    (c) Method in [5], PSNR = 24.59    (d) Our method, PSNR = 24.67

**Fig. 4**. Deconvolution of *Crym* (cropped) degraded by Gaussian blur ($\sigma^2=0.25$) and PG noise ($\alpha=4.25, \mu_\text{n}=0, \sigma_\text{n}=25.5$).

**Real microscopy images.** In practical applications, when the noise parameters are not available, they can be directly estimated from the original images using different methods (*e.g.*, [16, 17]). We performed joint super-resolution (factor of two), deconvolution, and denoising on real microscopy images of telomeres acquired with an easySTED system [18]. Examples are shown in Fig. 6. Noise parameters $\alpha \approx 3.2$ and $\sigma_\text{n} \approx 4.9$ were estimated using [17]. It can be seen that the noise as well as the blur have been significantly reduced. The resolution of the resulting images after applying our joint method is a factor of two higher compared to the original images. We employed these images for segmentation and shape analysis of telomeres using the model fitting approach in [19]. The model in this approach is based on a Fourier representation, and by fitting the model to an image the Fourier coefficients are determined. We applied the model fitting approach both to the original images and the high resolution images. It turned out that for the high resolution images from our joint method,



(a) Downsampled with noise, (128×128)    (b) Restored, (256×256), PSNR = 24.35    (c) Restored, (256×256), PSNR = 24.63

**Fig. 5**. Super-resolution (2x) and denoising of *Crym* using our method. PG noise ($\alpha=1, \mu_\text{n}=0, \sigma_\text{n}=10$) is applied to the downsampled image. *(b)* Denoising followed by bicubic interpolation; *(c)* Joint super-resolution and denoising. PSNR is computed based on the original image.
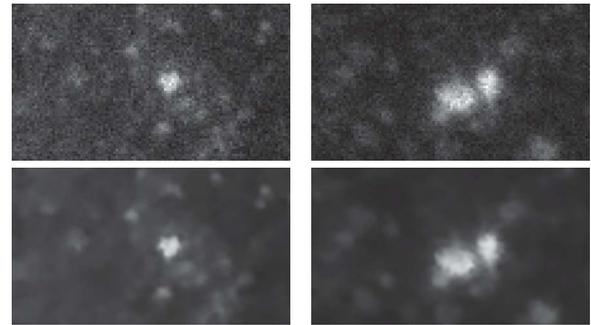


**Fig. 6**. Super-resolution (2x), deconvolution, and denoising of STED microscopy images using our method. *(Top)* original images; *(Bottom)* restored images. Noise parameters are estimated using [17]: $\alpha \approx 3.2$ and $\sigma_\text{n} \approx 4.9$.

the Fourier coefficients reflecting the shape were determined more robustly and accurately compared to using the original images. This is important for distinguishing different experimental conditions.

## 4. SUMMARY

We introduced a Bayesian method for joint super-resolution, deconvolution, and denoising of images with mixed Poisson-Gaussian noise. Degraded images are restored using MMSE estimation. Our main contributions are: 1) Exploration of the statistics of Poisson-Gaussian noise and usage of mixtures of Gaussians to approximate the likelihood; 2) Use of a generative probabilistic image prior; additional parameters are not needed; 3) Design of an efficient Gibbs sampler for inference to determine the MMSE estimate; 4) Integration of super-resolution into our model. Note that our method uses an application-neutral generative image prior, and thus can be straightforwardly adapted to image restoration problems with arbitrary linear operator as well as other types of noise.

# 5. REFERENCES

[1] F. Luisier, T. Blu, and M. Unser, "Image denoising in mixed Poisson-Gaussian noise," *IEEE Trans. Image Process.*, vol. 20, no. 3, pp. 696–708, 2011.

[2] M. Mäkitalo and A. Foi, "Optimal inversion of the generalized Anscombe transformation for Poisson-Gaussian noise," *IEEE Trans. Image Process.*, vol. 22, no. 1, pp. 91–103, 2013.

[3] S. A. Haider, A. Cameron, P. Siva, D. Lui, M. J. Shafiee, A. Boroomand, N. Haider, and A. Wong, "Fluorescence microscopy image noise reduction using a stochastically-connected random field model," *Scientific Reports*, vol. 6, no. 20640, 2016.

[4] A. Jezierska, E. Chouzenoux, J.-C. Pesquet, and H. Talbot, "A primal-dual proximal splitting approach for restoring data corrupted with Poisson-Gaussian noise," in *Proc. IEEE Int. Conf. on Acoustics, Speech, and Signal Process. (ICASSP)*, 2012.

[5] E. Chouzenoux, A. Jezierska, J.-C. Pesquet, and H. Talbot, "A convex approach for image restoration with exact Poisson-Gaussian likelihood," *SIAM Journal on Imaging Sciences*, vol. 8, no. 4, pp. 2662–2682, 2015.

[6] J. li, Z. Shen, R. Yin, and X. Zhang, "A reweighted L2 method for image restoration with Poisson and mixed Poisson-Gaussian noise," *Inverse Problems and Imaging*, vol. 9, no. 3, pp. 875–894, 2015.

[7] B. Bajic, J. Lindblad, and N. Sladoje, "Blind restoration of images degraded with mixed Poisson-Gaussian noise with application in transmission electron microscopy," in *Proc. IEEE Int. Symp. on Biomed. Imag. (ISBI)*, 2016.

[8] J. Li, F. Luisier, and T. Blu, "PURE-LET image deconvolution," *IEEE Trans. Image Process.*, vol. 27, no. 1, pp. 92–105, 2018.

[9] Y. Marnissi, Y. Zheng, E. Chouzenoux, and J.-C. Pesquet, "A variational Bayesian approach for image restoration. Application to image deblurring with Poisson-Gaussian noise," *IEEE Trans. Comput. Imaging*, vol. 3, no. 4, pp. 722–737, 2017.

[10] S. Gazagnes, E. Soubies, and L. Blanc-Feraud, "High density molecule localization for super-resolution microscopy using CEL0 based sparse approximation," in *Proc. IEEE Int. Symp. on Biomed. Imag. (ISBI)*, 2017.

[11] U. Schmidt, Q. Gao, and S. Roth, "A generative perspective on MRFs in low-level vision," in *Proc. IEEE Conf. on Comp. Vis. and Pat. Recog. (CVPR)*, 2010.

[12] U. Schmidt, K. Schelten, and S. Roth, "Bayesian deblurring with integrated noise estimation," in *Proc. IEEE Conf. on Comp. Vis. and Pat. Recog. (CVPR)*, 2011.

[13] Q. Gao and S. Roth, "How well do filter-based MRFs model natural images?," in *Pattern Recognition, Proc. DAGM-Symp.* 2012, vol. 7476 of *LNCS*, pp. 62–72, Springer.

[14] G. Papandreou and A. L. Yuille, "Gaussian sampling by local perturbations," in *Adv. in Neur. Inf. Proc. Sys. (NIPS)*, 2010.

[15] D. Chen, "Regularized generalized inverse accelerating linearized alternating minimization algorithm for frame-based Poissonian image deblurring," *SIAM Journal on Imaging Sciences*, vol. 7, no. 2, pp. 716–739, 2014.

[16] A. Jezierska, J.-C. Pesquet, H. Talbot, and C. Chaux, "Iterative Poisson-Gaussian noise parametric estimation for blind image denoising," in *Proc. IEEE Int. Conf. on Image Proc. (ICIP)*, 2014.

[17] M. Mäkitalo and A. Foi, "Noise parameter mismatch in variance stabilization, with an application to Poisson-Gaussian noise estimation," *IEEE Trans. Image Process.*, vol. 23, no. 12, pp. 5348–5359, 2014.

[18] F. Görlitz, P. Hoyer, H. J. Falk, L. Kastrup, J. Engelhardt, and S. W. Hell, "A STED microscope designed for routine biomedical applications," *Progress In Electromagnetics Research*, vol. 147, pp. 57–68, 2014.

[19] S. Eck, S. Wörz, K. Müller-Ott, M. Hahn, A. Biesdorf, G. Schotta, K. Rippe, and K. Rohr, "A spherical harmonics intensity model for 3D segmentation and 3D shape analysis of heterochromatin foci," *Medical Image Analysis*, vol. 32, pp. 18–31, 2016.